ELSEVIER

J. Non-Newtonian Fluid Mech., 80 (1999) 251–268

Journal of Non-Newtonian Fluid Mechanics

Structure of the spectrum in zero Reynolds number shear flow of the UCM and Oldroyd-B liquids

Helen J. Wilson [a], Michael Renardy [b], Yuriko Renardy [b,*]

[a] *Department of Applied Mathematics and Theoretical Physics, University of Cambridge, Cambridge CB3 9EW, UK*
[b] *Department of Mathematics and ICAM, Virginia Polytechnic Institute and State University, Blacksburg, Virginia 24061-0123, USA*

Received 04 February 1998

Abstract

We provide a mathematical analysis of the spectrum of the linear stability problem for one and two layer channel flows of the upper-convected Maxwell (UCM) and Oldroyd-B fluids at zero Reynolds number. For plane Couette flow of the UCM fluid, it has long been known (Gorodstov and Leonov, J. Appl. Math. Mech. (PMM) 31 (1967) 310) that, for any given streamwise wave number, there are two eigenvalues in addition to a continuous spectrum. In the presence of an interface, there are seven discrete eigenvalues. In this paper, we investigate how this structure of the spectrum changes when the flow is changed to include a Poiseuille component, and as the model is changed from the UCM to the more general Oldroyd-B. For a single layer UCM fluid, we find that the number of discrete eigenvalues changes from two in Couette flow to six in Poiseuille flow. The six modes are given in closed form in the long wave limit. For plane Couette flow of the Oldroyd-B fluid, we solve the differential equations in closed form. There is an additional continuous spectrum and a family of discrete modes. The number of these discrete modes increases indefinitely as the retardation time approaches zero. We analyze the behavior of the eigenvalues in this limit.

Keywords: Poiseuille component; Maxwell liquid; Couette flow

1. Introduction

A number of papers have appeared on the numerical computation of the discrete and continuous spectra of Couette and Poiseuille flows of the upper convected Maxwell and Oldroyd-B fluids [1–3]. Based on these computational results, the question of the stability at zero Reynolds number has largely been settled. However, questions have been raised about the unusual features, namely, modes which appear or disappear near continuous spectra, the

* Corresponding author. Fax: +1 540 231 5960.

0377-0257/99/$ - see front matter
PII S0377-0257(98)00087-1

discrete modes whose numbers vary with fluid parameters, etc. Mathematically, the intriguing feature of Couette flow of the upper convected Maxwell liquid in both one and two layers is that the discrete modes are determined by polynomial equations, rather than transcendental equations of, e.g. Newtonian flow [4]. The question arises whether this feature persists when the flow and model are changed. In this paper, we provide a cohesive analysis for the entire spectrum and explain the origins of each component.

The linear stability problem for plane Couette flow of the UCM fluid at zero Reynolds number was analyzed in [5]. It was found that, in addition to a continuous spectrum, there are precisely two discrete eigenvalues for any given streamwise wave number. These two eigenvalues, and their associated eigenfunctions, can be found explicitly. In two-layer Couette flow of the UCM fluid, seven discrete eigenvalues exist. For short wavelength, they separate into two modes which are localized at the walls and five which are localized at the interface [6].

These features are quite unusual and must be linked to rather special algebraic properties of the underlying equations. It is therefore of interest to see how the nature of the spectrum changes when either the constitutive model or the flow becomes perturbed. In this paper, we investigate what happens if the flow is allowed to have a Poiseuille component or the model is generalized to the Oldroyd-B fluid.

The equations governing the linear stability problem are a system of linear ordinary differential equations; by a process of elimination they can be combined into a single ordinary differential equation (ODE). The continuous spectra are associated with regular singular points of this ODE. Generically, the solutions of an ODE near a regular singular point involve fractional powers and/or logarithms, i.e. in the complex plane they are multivalued. For this reason, continuous spectra are usually branch cuts for the equation which determines the eigenvalues. Nevertheless, for Couette flow of the UCM fluid, the eigenvalues are determined by polynomials which have no branch cuts. Indeed, the analysis of singular points in Section 3 will show that all solutions of the differential equation are analytic, even though there is a singular point.

For Couette flow of the Oldroyd-B fluid (see closed form solutions in Section 4), there are two parts of the continuous spectrum, the part which is already there in the UCM case, and a 'new' part which moves out to infinity as the retardation time tends to zero. Rather surprisingly, it turns out that, even for the Oldroyd B fluid, the 'UCM' part of the continuous spectrum remains qualitatively the same as in the UCM fluid. On the other hand, the 'new' part of the continuous spectrum is a branch cut. In this case, discrete eigenvalues can appear or disappear as they move from one Riemann sheet to another across the branch cut. This is further documented in Sections 6 and 7, where we find that discrete eigenvalues emerge from this branch cut as we change the value of the retardation time, with the number of eigenvalues increasing to infinity as the retardation time approaches zero.

These features change if the flow includes a Poiseuille component. The continuous spectrum for the UCM model now becomes a branch cut, allowing the number of discrete modes to change if eigenvalues cross this branch cut. Indeed, we find that as we change from Couette to Poiseuille flow, the number of discrete eigenvalues changes from two to six. The number six is derived analytically for the long wave limit in Section 5. In Sections 6 and 7, we interpret the salient features of computational results using both a spectral code and a shooting code in the light of the analytical results.

2. Governing equations

We consider the linear stability of parallel shear flow of two Oldroyd-B fluids arranged in layers. We state our equations in dimensionless form. The flow domain is $0 < z < 1$; fluid 1 occupies the region $0 < z < l_1$ and fluid 2 occupies $l_1 < z < 1$. Fluid i has total viscosity μ_i and solvent viscosity η_i; the dimensionless ratios are $\beta_i = \eta_i/\mu_i$, $0 \leq \beta_i < 1$ and $m = \mu_1/\mu_2$. The scales for nondimensionalization are the total width l^* of the channel for lengths, the velocity U_i at the interface for velocities, and $\mu_1 U_i/l^*$ for stresses. For each fluid, we define a dimensionless Weissenberg number $W_i = \lambda_i U_i/l^*$, where λ_i is the relaxation time of fluid i. We note that $W_i\beta_i$ is the dimensionless retardation time, and we shall refer to β_i as a retardation parameter.

The dimensionless equation of motion for fluid i is

$$\operatorname{div} \mathbf{T} - \nabla p + \beta_i \frac{\mu_i}{\mu_1} \Delta \mathbf{u} = 0. \tag{1}$$

In addition, we have the incompressibility condition

$$\operatorname{div} \mathbf{u} = 0, \tag{2}$$

and the UCM constitutive law

$$W_i\left(\frac{\partial \mathbf{T}}{\partial \mathbf{t}} + (\mathbf{u} \cdot \nabla) - (\nabla \mathbf{u})\mathbf{T} - \mathbf{T}(\nabla \mathbf{u})^T\right) + \mathbf{T} = \frac{\mu_i(1-\beta_i)}{\mu_1}(\nabla \mathbf{u} + (\nabla \mathbf{u})^T). \tag{3}$$

At the interface, we have continuity of velocity and traction and the kinematic free surface condition.

We consider linearized perturbations of the combined Couette-Poiseuille flow

$$U(z) = \begin{cases} -Gz^2/2 + c_1 z, & 0 < z < l_1, \\ -mG(z-1)^2/2 + c_2(z-1) + U_\mathrm{p} & l_1 < z < 1. \end{cases} \tag{4}$$

Here

$$\begin{aligned} c_1 &= 1/l_1 + Gl_1/2, \\ c_2 &= m(-G + c_1), \\ U_\mathrm{p} &= 1 + m(1-l_1)/l_1 - mG(1-l_1)/2, \end{aligned} \tag{5}$$

and G is the imposed (dimensionless) pressure gradient. The polymer stress in the base flow is

$$\mathbf{T} = \begin{pmatrix} C_1 & C_2 \\ C_2 & 0 \end{pmatrix}, \tag{6}$$

where

$$C_1 = (1-\beta_i)\left(\frac{\mu_i}{\mu_1}\right)2W_i[U'(z)]^2, \qquad C_2 = (1-\beta_i)\frac{\mu_i}{\mu_1}U'(z). \tag{7}$$

We linearize at this base flow and seek perturbation proportional to $\exp(i\alpha x + \sigma t)$. With a prime denoting $\mathrm{d}/\mathrm{d}z$, the equations for the linearized perturbations are the following. The equation of motion reads

$$i\alpha(T_{11}-p)+T'_{12}+\beta_i\frac{\mu_i}{\mu_1}(u''-\alpha^2u)=0,\qquad i\alpha T_{12}+T'_{22}-p'+\beta_i\frac{\mu_i}{\mu_1}(v''-\alpha^2v)=0. \tag{8}$$

The incompressibility condition is

$$i\alpha u+v'=0, \tag{9}$$

and the constitutive equations become

$$W_i((\sigma+i\alpha U(z))T_{11}+C'_1(z)v-2C_1(z)i\alpha u-2C_2(z)u'-2U'(z)T_{12})$$

$$+T_{11}=2(1-\beta_i)\frac{\mu_i}{\mu_1}i\alpha u,$$

$$W_i((\sigma+i\alpha U(z))T_{12}+C'_2(z)v-C_1(z)i\alpha v-U'(z)T_{22})+T_{12}$$

$$=(1-\beta_i)\frac{\mu_i}{\mu_1}(u'+i\alpha v),$$

$$W_i((\sigma+i\alpha U(z))T_{22}-2C_2i\alpha v)+T_{22}=2(1-\beta_i)\frac{\mu_i}{\mu_1}v'. \tag{10}$$

The linearized interface conditions are: at $z=l_1$, the continuity of velocity

$$[u]+h[U']=[v]=0, \tag{11}$$

continuity of traction

$$[T_{12}]-i\alpha h[C_1]+\left[\beta_i\frac{\mu_i}{\mu_1}(u'+i\alpha v)\right]=[T_{22}-p]+2\left[\beta_i\frac{\mu_i}{\mu_1}v'\right]=0, \tag{12}$$

and the kinematic free surface condition

$$(\sigma+i\alpha U(l_1))h-v=0. \tag{13}$$

Here, h is the perturbation to the interface position and $[\,\cdot\,]$ denotes the jump of a quantity across the interface, i.e. the value in fluid 1 minus the value in fluid 2.

Finally, we must satisfy the boundary conditions

$$u=v=0 \tag{14}$$

on the walls $z=0$ and $z=1$.

3. Singular points

We can combine the differential system (Eqs. (8)–(10)) into a single equation for v by eliminating u from Eq. (9), p from the first equation of Eq. (8), and T_{11}, T_{12}, T_{22} from Eq. (10).

The result is a fourth order ordinary differential equation for v. The solutions of this differential equation are analytic functions of z and σ except possibly at singular points where the coefficient of the highest derivative vanishes. These singular points occur when either

$$1 + W_i(\sigma + i\alpha U(z)) = 0, \tag{15}$$

or

$$\frac{1}{\beta_i} + W_i(\sigma + i\alpha U(z)) = 0. \tag{16}$$

For plane Couette flow of the upper convected Maxwell fluid, the differential equation can be solved explicitly as shown by Gorodtsov and Leonov [5]. Their explicit solution shows that the solutions of the differential equation are analytic, even at the singular points. Indeed, the singular points are regular singular points, therefore, a local expansion (with respect to z) of solutions can be found using Frobenius theory. The roots of the indicial equation are 0, 1, 3 and 4 [2], i.e. all integers. In addition, it turns out that none of the solutions involve logarithmic terms, even though the roots of the indicial equation differ by an integer. Consequently, we can find four linearly independent solutions of the differential equation, which depend analytically on σ and z for all σ and z. By inserting a linear combination of these solutions into the boundary and interface conditions, and setting the resulting determinant equal to zero, we obtain an entire function of σ, and the eigenvalues are the zeros of this function. Indeed, this entire function turns out to be a polynomial. For single layer Couette flow, the polynomial is of degree two, and for two-layer flow, it is of degree seven. In the limit $\alpha \to \infty$, the seven roots can be divided into two modes localized at the wall, which correspond to the Gorodtsov-Leonov modes which already exist in the single-layer case and five modes which are localized at the interface [6].

We have extended the study of the local behavior near the singular points to the case of Couette flow of the Oldroyd-B fluid. The calculations were done using Mathematica, and we only report the results. All the singular points are still of regular singular type. For the singular points given by Eq. (15), the roots of the indicial equation are still 0, 1, 3 and 4, and all solutions are analytic. For the singular points given by Eq. (16), the roots of the indicial equation are 0, 1, 2 and $3 - 2/\beta_i$. The solutions corresponding to the first three roots are analytic, i.e. again there are no logarithmic terms even though the difference between two roots is an integer. On the other hand, $3 - 2/\beta_i$ is generally not an integer, and hence there is a solution involving a fractional power of z (and also a fractional power of σ since the solutions depend on σ and z through the combination $\sigma + i\alpha U(z)$). As a consequence, the function determining the eigenvalues ceases to be analytic for all σ and has a branch cut along the line where Eq. (16) holds for some $z \in (0, 1)$. On the other hand, the line where Eq. (15) holds for some $z \in (0, 1)$ is not a branch cut, even though it is part of the continuous spectrum. The distinction is important, as eigenvalues can emerge from or disappear through a branch cut as parameters change; we shall see examples in the results below. On the other hand, this is not possible for parts of the continuous spectrum which are not branch cuts.

If the flow is changed to combined Couette-Poiseuille flow, both parts of the continuous spectrum become branch cuts.

4. Couette flow of the Oldroyd B fluid

4.1. Closed form solution

We consider the case of plane Couette flow, and solve the system of differential Eqs. (8)–(10) in closed form. For the UCM case, this was done in [5]. Without loss of generality, we set $U(z) = z$, and $\mu_i = \mu_1$, and we write W for W_i and β for β_i. The equations can be combined into one fourth order differential equation as outlined in the preceding section. We solve for the four linearly independent solutions. With

$$S = 1 + W(\sigma + i\alpha z), \tag{17}$$

the result is [7]:

$$(1-\beta)\Delta[S^{-1}(\Delta v + 2Wi\alpha v' - 2W^2\alpha^2 v)] + \beta\Delta^2 v = 0. \tag{18}$$

Here Δ is the Laplace operator $\Delta v = v'' - \alpha^2 v$. The key here is that two of the Gorodtsov-Leonov solutions for the UCM case $\Delta[S^{-1}(\Delta v + 2Wi\alpha v' - 2W^2\alpha^2 v)] = 0$ also satisfy $\Delta^2 v = 0$, and therefore carry over to the Oldroyd B case, since the extra term in Eq. (18) is zero. Consequently, two linearly independent solutions for Eq. (18) are given by

$$v = \exp(\pm\alpha z)(\sigma + i\alpha z). \tag{19}$$

We next consider the remaining two solutions, which satisfy

$$(1-\beta)(\Delta v + 2iW\alpha v' - 2\alpha^2 W^2 v) + \beta S\Delta v = 0. \tag{20}$$

This equation is of confluent hypergeometric type, and hence its solutions are transcendental. The general solution is

$$v = \mathrm{e}^{-\alpha z}\left[A\,{}_1F_1\left((1-iW)\left(\frac{1}{\beta}-1\right), \frac{2}{\beta}-2, -\frac{2i}{\beta W}(1+\beta W(\sigma+i\alpha z))\right)\right.$$
$$\left. + BU\left((1-iW)\left(\frac{1}{\beta}-1\right), \frac{2}{\beta}-2, -\frac{2i}{\beta W}(1+\beta W(\sigma+i\alpha z))\right)\right], \tag{21}$$

where A and B are constants. Note that ${}_1F_1(a, b, c)$ is an entire function of c with a, b fixed, while the only singularity of $U(a, b, c)$ (again as a function of c with fixed a and b) is at $c = 0$. Therefore, only the second contribution in Eq. (21) has a singularity, and this singularity is at the point where

$$1 + \beta W(\alpha + i\alpha z) = 0, \tag{22}$$

Moreover, the behavior near this singularity is proportional to [8]

$$(1 + \beta W(\sigma + i\alpha z))^{3-2/\beta}, \tag{23}$$

in agreement with the discussion of the previous section. Finally, the general solution for the eigenmode is a linear combination of functions appearing in Eqs. (19) and (21). This can now be substituted into the remaining boundary conditions to solve for the eigenvalues, leading to a transcendental equation for the eigenvalues with a branch cut along the line $\mathrm{Re}(\sigma) = -1/(\beta W)$,

$-\alpha \leq \mathrm{Im}(\alpha) \leq 0$. It is found that apart from the two strips of continuous spectra and the two Gorodtsov-Leonov modes, there is a string of discrete eigenvalues which appear in the Oldroyd-B model that are not there in the UCM model. To analyze these modes, we shall pursue a simplified equation for small β rather than using the solution in terms of hypergeometric functions.

4.2. The limit of small β

We focus on the family of discrete modes which are present in the Oldroyd-B model but not in the UCM. To see how the transition comes about, we need to examine the case of β small. The following substitutions focus the analysis:

$$\sigma = \frac{1}{W\beta}(-1+q), \tag{24}$$

so that

$$S^{-1} = \frac{\beta}{-1+q} + O(\beta)^2. \tag{25}$$

We note that in this approximation, in addition to β being small, we also need $\alpha\beta$ to be small, due to the presence of the term $Wi\alpha z$ in S, which is assumed small relative to $W\sigma$. The case where $\alpha \to \infty$ and $\beta \to 0$ simultaneously would require a different analysis. We use Eq. (25) in Eq. (18), retaining only terms of order β. The result is

$$\frac{1}{-1+q}\Delta(\Delta v + 2Wi\alpha v' - 2W^2\alpha^2 v) + \Delta^2 v = 0. \tag{26}$$

This is an equation with constant coefficients, which we can solve in closed form. We insert the result into the boundary conditions for single-layer flow: $v(0) = v'(0) = v(1) = v'(1) = 0$. The resulting characteristic equation is of the form

$$\exp(2i\alpha W/q) = f(q), \tag{27}$$

where $f(q)$ is analytic in a neighborhood of $q = 0$, and $|f(0)| = 1$. We can take the logarithm to find that

$$2i\alpha W = q\,\log(f(0)) + O(q^2). \tag{28}$$

If we neglect the $O(q^2)$ term, we find $q = 2i\alpha W/\log f(0)$. For this to be consistent, q should be small so we can justify neglecting q^2. Note that the logarithm has infinitely many values. If we choose a branch of $\log(f(0))$ such that $|\log(f(0))|$ is sufficiently large, then we can use perturbation theory to show that Eq. (28) has a root which is close to $2i\alpha W/\log(f(0))$. In this fashion, we obtain infinitely many solutions of Eq. (27). Hence, in the limit $\beta \to 0$, there should be an infinite number of discrete modes. These move in from infinity as β increases. Since the log function can be either positive or negative imaginary, the q can be of either sign. Hence, these modes manifest themselves in the numerical simulations of Sections 6 and 7 as 'strings' of discrete eigenvalues on both sides of the continuous spectrum.

5. Long wave asymptotics for single-layer Poiseuille flow of the UCM fluid

We now consider the plane Poiseuille flow of a single fluid in the limit of small α. To exploit the symmetry of the Poiseuille flow, we choose the flow domain to be $-1<z<1$; the base flow is given by $U(z)=1-z^2$, We consider Eqs. (8)–(10) subject to the boundary conditions $u=v=0$ at $z=\pm 1$, where the fluid consists of a single layer UCM, i.e. $\mu_i/\mu_1=1$, $\beta_i=0$, and we write W for W_i. For small α, we can set $\sigma=-1/W+\alpha\tau$, $u=\alpha\tilde{u}$, $v=\alpha^2\tilde{v}$, $T_{22}=\alpha\tilde{T}_{22}$, $T_{12}=\tilde{T}_{12}$, $T_{11}=\tilde{T}_{11}/\alpha$. At leading order, this leads to the system

$$\begin{aligned}
&(\tau+iU(z))\tilde{T}_{11}-2U'(z)\tilde{T}_{12}=0,\\
&W((\tau+iU(z))\tilde{T}_{12}-U'(z)\tilde{T}_{22})-\tilde{u}'=0,\\
&W((\tau+iU(z))\tilde{T}_{22}-2\tilde{v}'=0,)\\
&i\tilde{u}+\tilde{v}'=0,\\
&i\tilde{T}'_{11}+\tilde{T}''_{12}=0.
\end{aligned}\tag{29}$$

Successive elimination of variables leads to the single equation

$$16z\tilde{v}'+(2z^2+6-6i\tau)\tilde{v}''-4z(-1+z^2-i\tau)^2\tilde{v}'''+(z^2-1+i\tau)^2\tilde{v}^{(4)}=0.\tag{30}$$

This equation has the obvious solution $v_1(z)=1$, as well as the polynomial solution

$$v_2(z)=-(i+\tau)^2z+\frac{2}{3}i(i+\tau)z^3+\frac{1}{5}z^5.\tag{31}$$

We can then use the reduction of order method to reduce the differential equation to second order. Mathematica yields the additional solutions

$$\begin{aligned}
v_3(z)=&\frac{(-1)^{1/4}}{\sqrt{i+\tau}}(-15i(i+\tau)^2z-10(i+\tau)z^3+3iz^5)\arctan\left(\frac{(-1)^{3/4}z}{\sqrt{i+\tau}}\right)\\
&+3z^2(-3+3i\tau+z^2)-4i(i+\tau)^2\arctan(\tau-iz^2)\\
&+2(i+\tau)^2\ln(-1-(\tau-iz^2)^2),\\
v_4(z)=&-480(-1)^{1/4}(i+\tau)^{5/2}\arctan\left(\frac{(-1)^{3/4}z}{\sqrt{i+\tau}}\right)\\
&+z\Bigg[-1680(i+\tau)^2+340i(i+\tau)z^2+36z^4\\
&+15(15(i+\tau)^2+10(1-i\tau)z^2-3z^4)*\left(2i\arctan\left(\frac{1-z^2}{\tau}\right)+\ln(\tau^2+(-1+z^2)^2)\right)\Bigg].
\end{aligned}\tag{32}$$

Due to the symmetry of the Poiseuille flow, the eigenfunctions are either varicose modes for which v is odd or snake modes for which v is even. In the first case, v is a superposition of v_2 and v_4. By taking such a superposition and imposing the boundary conditions $v(1)=v'(1)=0$, we obtain the characteristic equation

$$f(\tau)=-80+440i\tau+566\tau^2-95i\tau^3+120\tau^4$$

$$+ 120(-1)^{1/4}\tau^2(i+\tau)^{5/2}\arctan\left(\frac{(-1)^{3/4}}{\sqrt{i+\tau}}\right) = 0. \tag{33}$$

For the snake modes, v is a superposition of v_1 and v_3, and the characteristic equation becomes

$$g(\tau) = 2i + 7\tau - 5i\tau^2 + 3(-1)^{3/4}\tau^2\sqrt{i+\tau}\arctan\left(\frac{(-1)^{3/4}}{\sqrt{i+\tau}}\right) = 0. \tag{34}$$

The functions f and g each have a branch cut extending from $-i$ to 0.

We next determine the number of discrete eigenvalues by using the argument principle. We note that for large τ, f behaves like τ^3, while g behaves like τ^2 Hence, with C denoting the circle $|\tau| = R$ and R chosen sufficiently large, we have

$$\int_C f'(\tau)/f(\tau)\mathrm{d}\tau = 6\pi i, \qquad \int_C g'(\tau)/g(\tau) = 4\pi i. \tag{35}$$

On the other hand, we can evaluate the same integral on a loop which goes around the branch cut at a close distance; we chose the curve Γ given by

$$\tau(\theta) = -i/2 + 0.01\cos(\theta) + 0.51i\sin\theta, \quad 0 \le \theta \le 2\pi. \tag{36}$$

A schematic diagram showing the location of C and Γ is given in Fig. 1. Numerical integration using Mathematica's routine NIntegrate yields

$$\int_\Gamma f'(\tau)/f(\tau)\mathrm{d}\tau = -2\pi i,$$
$$\int_\Gamma g'(\tau)/g(\tau)\mathrm{d}\tau = 0. \tag{37}$$

By the argument principle, the difference between the integral over C and the integral over Γ is $2\pi i$ times the number of zeros in between. Comparing Eqs. (35) and (37), these differences are $8\pi i$ and $4\pi i$, respectively. Hence, f has four zeros, and g has two. Consequently, there must be four eigenvalues belonging to varicose modes and two belonging to snake modes.

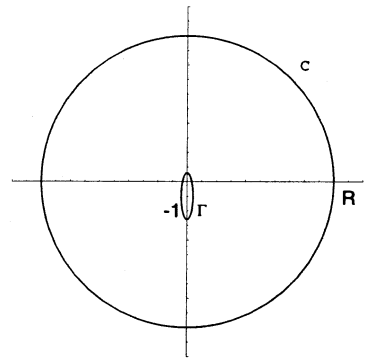

Fig. 1. Contours for integration.

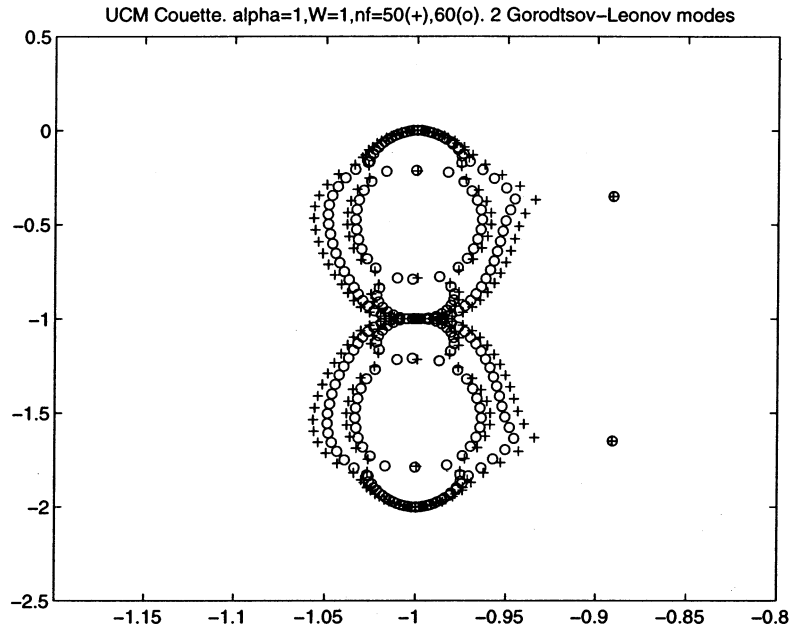

Fig. 2. Eigenspectrum for Couette flow of a UCM fluid using 50 and 60 Chebyshev modes.

6. Numerical results for single-layer flow

6.1. Couette

The numerical code we used is written for a two-layer flow [9], and we therefore treat the single-layer problem as a double-layer problem with $l_1 = 0.5$ and both fluids equal. Thus, in keeping with the non-dimensionalization of the velocity with respect to U_i of Section 2, the base flow has the form $U(z) = 2z$ and z ranges from 0 to 1. In plane Couette flow, the complete eigenspectrum is known for the UCM fluid [5]. It consists of a continuous spectrum $-\alpha U(\text{wall}) \leq \sigma_i \leq 0$, $\sigma_r = -1/W$ and two discrete modes, which, by symmetry considerations, have equal real parts while their imaginary parts are balanced around the line corresponding to the centre of the channel: $\sigma_i = -\alpha \pm \theta$ for some θ. A numerical example of this spectrum is shown in Fig. 2, where $\alpha = 1$ and the two modes are at $\sigma_i \approx -0.3$ and -1.7. The discretization is based on the Chebyshev-tau method. The figure shows the results for two different refinements of discretization; the number *nf* in the figure denotes the number of Chebyshev polynomials used in each layer to approximate the streamfunction. It is meaningful to show results for two different values of *nf* as the method converges faster for the smoother solutions; the unconverged eigenvalues belong to the more singular solutions. Fig. 2 clearly shows the two Gorodtsov-Leonov eigenvalues which do not move in location as *nf* is changed. On the other hand, the continuous spectrum is poorly resolved. While it is theoretically a line segment, it shows up in the numerical results as a 'balloon' (or in this case a double-balloon, since we are treating the problem as a two-layer flow). A very high resolution would be required to narrow the width of this balloon; note that the balloon for $nf = 60$ is only slightly narrower than that for $nf = 50$.

To move to the more general Oldroyd-B fluid, in our formulation we increase the parameter β. Fig. 3 shows the different parts of the spectrum at $W=1$, $\alpha=1$, $\beta=0.2$. As above, we see that the discrete modes are well converged, while the continuous spectra show up as balloons. We note that Fig. 3(a) shows a discrete eigenvalue at $-i$: this is an interfacial mode which is introduced artificially by treating the single-layer flow as a two-layer flow. We can now distinguish two parts of the spectrum: the 'old' spectrum, which arises by continuation from the case of the UCM fluid (Fig. 3(c)), and a 'new' spectrum, which moves out to infinity in the limit $\beta \to 0$ (Fig. 3(b)) We find that the 'old' spectrum, including the two Gorodtsov-Leonov modes, is not strongly affected by the addition of a solvent viscosity to the fluid. The new part of the spectrum includes a second continuous spectrum, with the same range of imaginary parts as the first, but with real part $\sigma_r = -1/(\beta W)$, which comes in from $-\infty$ as β increases from zero. It carries with it a string of discrete roots, which all have imaginary part $\sigma_i = -\alpha$ (Fig. 3(b)). Their real parts are distributed both larger and smaller than the continuous spectrum; and their number decreases with increasing β. We note that the asymptotic analysis of Section 4.2 predicts an infinite number of discrete eigenvalues of the continuous spectrum for the limit when β approaches zero. From the numerical results, it appears that at any finite β, there is actually only a finite number of discrete modes, and each root in turn moves into the continuous spectrum as β is increased. For the example case $W=1$, $\alpha=1$, there are over 10 of these discrete eigenvalues at $\beta=0.1$ and only 2 by $\beta=0.3$.

If the wavenumber α is increased, we find that these extra discrete roots are no longer distributed evenly on both sides of the continuous spectrum. Rather they all shift to the left, i.e.

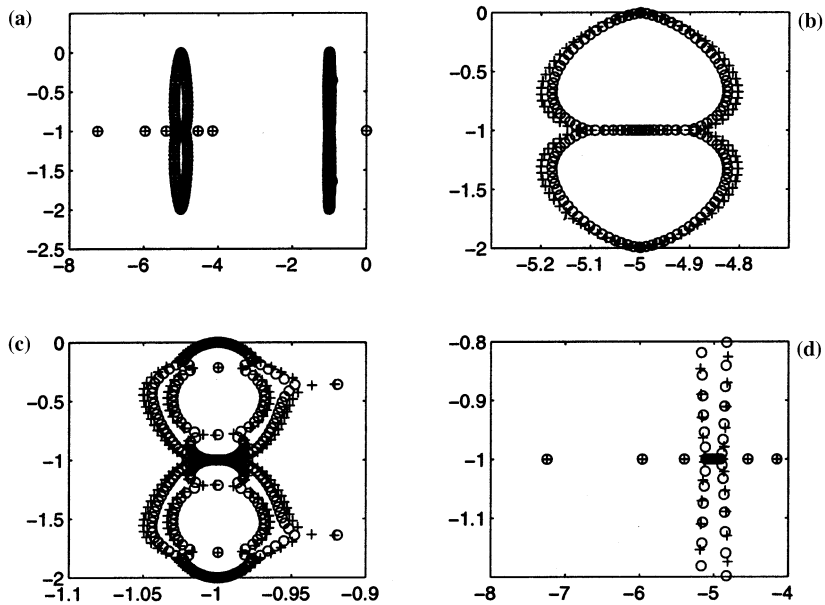

Fig. 3. Spectrum for Couette flow of an Oldroyd-B fluid. The parameters are $\alpha=1$, $\beta=0.2$, $W=1$. Results with 60 (crosses) and 70 (circles) Chebyshev modes are shown. (a) shows the entire spectrum for 60 and 70 Chebyshev modes; (b) and (c) are magnifications of the 'new' and 'old' continuous spectra, respectively; and (d) zooms in on the vertical scale of (b).

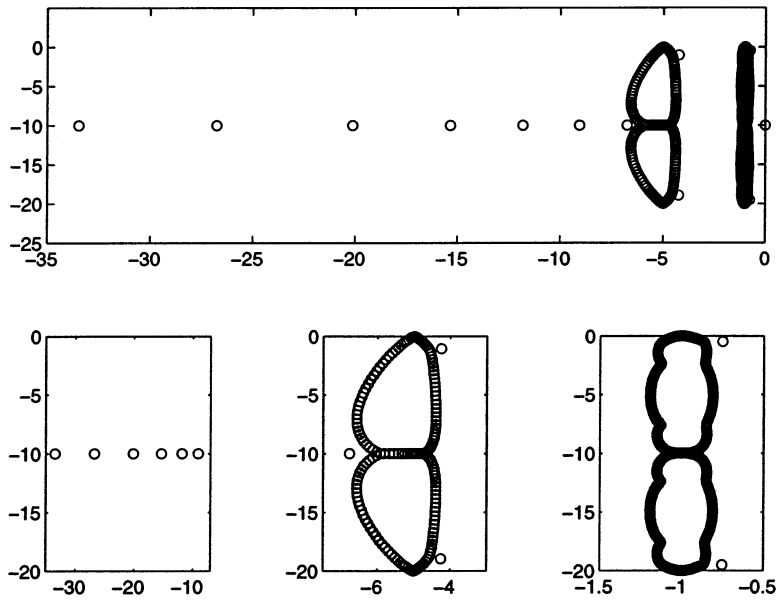

Fig. 4. Short-wave spectrum of an Oldroyd-B fluid in Couette flow. $\alpha = 10$, $\beta = 0.2$, $W = 1$.

they decay faster than the continuous spectrum. An example of this effect is shown in Fig. 4. We note that the analysis in Section 4.2 is for the limit $\beta \to 0$ when α is fixed and loses its validity if $\beta \to 0$ and $\alpha \to \infty$ at the same time.

6.2. Poiseuille

When the UCM fluid is studied in Poiseuille flow, the eigenspectrum consists, as above, of a continuous spectrum and a discrete spectrum. The continuous spectrum has decay rate $1/W$ and convects with the flow, so that its imaginary part obeys $-\alpha U(\text{centreline}) \leq \sigma_i \leq 0$. In keeping with the nondimensionalization of Section 2, the base velocity U at the centreline is 1. The discrete spectrum consists, for long waves, of four varicose or sausage-like modes and two sinuous or snake-like modes, as predicted in Section 5. Fig. 5 shows the spectrum for $W = 1$, obtained with the spectral scheme (o) together with results from a shooting scheme (*). The shooting method is as described in [10,11]. As the wavenumber increases, one of the varicose modes moves into the continuous spectrum and ceases to exist. This mode (found by a shooting method) is never very far from the continuous spectrum, and cannot be resolved by the spectral method. All six discrete modes are shown in Fig. 5 at a wavenumber $\alpha = 0.4$. We can see that the spectral method accurately resolves five of these modes, while the sixth one lies within the scatter of the continuous spectrum. It does, however, cause a slight distortion in the shape of the 'balloon'.

As the retardation parameter α is increased, there is again the 'UCM' part of the spectrum which arises by continuation from the UCM case, and a 'new' part which comes in from infinity. Fig. 6(a) shows a sample of the entire spectrum at $W = 1$. As was the case in Couette flow, the

'UCM' spectrum shown in Fig. 6(b) is largely unchanged. One of the five observable discrete modes moves into the continuous spectrum for moderate β (larger than ~ 0.4), however, the major changes are not in this area.

The second continuous spectrum, at real part $-1/(\beta W)$, appears exactly as it did in the Couette case; and brings with it a string of discrete modes as before. This is shown in Fig. 6(c) of the figure. However, the Poiseuille flow does not have the same symmetry properties as the Couette flow, and these modes do not all have the same imaginary part. Rather, they 'droop' on either side of the continuous spectrum. As β increases, these roots move into their continuous spectrum and their number decreases rapidly, from at least 16 at $\beta = 0.1$ to 6 at $\beta = 0.3$, and probably only one at $\beta = 0.5$.

We have also investigated the behavior of discrete modes in the UCM case as the wave number is varied. For long waves, we have four varicose and two sinuous modes. For short-wave perturbations, any eigenmode is expected to be localised, and the flow in a small locality is approximately simple shear, so we expect to see a Gorodtsov-Leonov mode at each wall. These two eigenmodes have the same eigenvalue, so one varicose and one sinuous mode may be constructed from them. It is of interest to see what happens to the remaining four modes as α becomes large.

Using the shooting method mentioned earlier, we trace the behaviour of the six long-wave roots as $0 < \alpha < \infty$. These results are shown in Fig. 7 for $W = 1$. Fig. 7(b) is a magnification of Fig. 7(a) to show the eigenvalues that remain bounded. At the limit $\alpha = 0$, all six roots coincide at $\sigma = -1/W$, which is the point $(-1, 0)$ in the figure. As expected, two roots, one varicose and one sinuous, tend to the Gorodtsov-Leonov value as $\alpha \to \infty$. These are denoted (o) in Fig. 7(b).

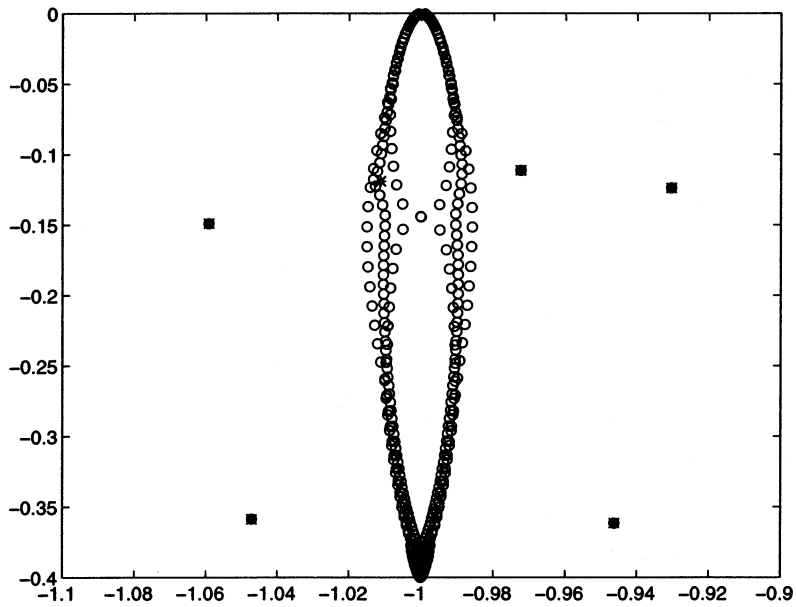

Fig. 5. Spectrum for Poiseuille flow of a UCM fluid, $W = 1$, $\alpha = 0.4$. Circles denote results obtained with 120 Chebyshev modes, while stars are discrete eigenvalues found by the shooting method.

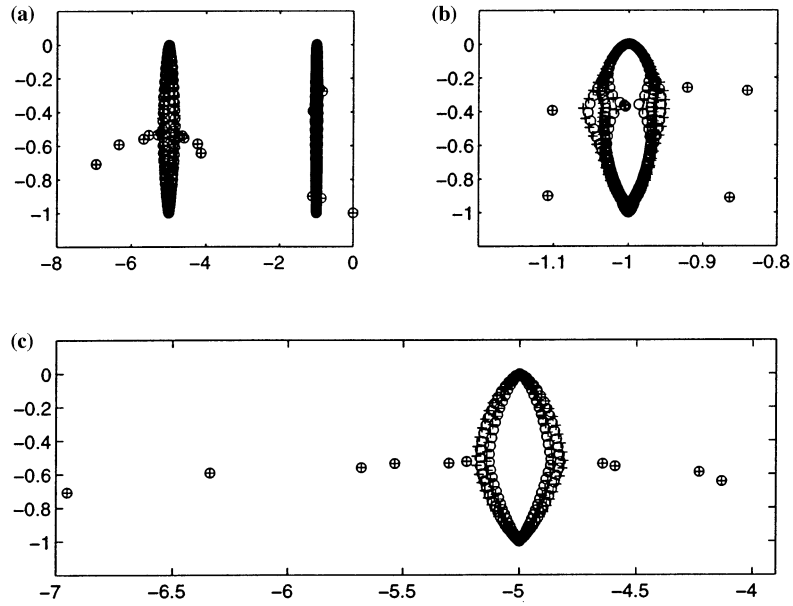

Fig. 6. Spectrum for Poiseuille flow of an Oldroyd-B fluid. (a) shows the entire spectrum; (b) and (c) show the 'UCM' and 'new' parts. The parameters are $\alpha = 1$, $\beta = 0.2$. Results are shown for 80 (crosses) and 90 (circles) Chebyshev modes.

Two of the other four (again, one sinuous and one varicose) cease to exist at some critical wavenumber when they encounter the continuous spectrum. These are denoted (*) in the figure. For the case shown, the critical wavenumbers are approximately $\alpha = 0.44$ for the varicose mode and $\alpha = 1.54$ for the sinuous one.

The remaining two roots, both of which are varicose, have convective part $\sigma_i \sim -\alpha$, and thus are convected with the fluid in the centre of the channel. They also remain stable, however, they are not available through the Gorodtsov-Leonov analysis due to being localized near the centre of the channel where the shear rate is zero.

6.3. Transition from Couette to Poiseuille

We now consider flows of the UCM fluid ($\beta = 0$) which are a combination of a Couette and Poiseuille component. For any such flow, there is one continuous spectrum and a small family of discrete eigenvalues. In each case the continuous spectrum is the same: the real part $\sigma_i = -1/W$ and the imaginary part ranges from 0 to $-\alpha U$ where U is the maximum base flow velocity anywhere in the channel.

For pure Couette flow the discrete spectrum consists of the two Gorodtsov-Leonov modes. As the Poiseuille component of the flow is increased, these two modes persist, one eventually becoming varicose in pure Poiseuille flow and the other sinuous. In our numerical simulations, we can observe three more modes appearing as the flow is changed from Couette to Poiseuille flow. We know that four exist, but one of the four remains too close to the continuous spectrum to be resolved numerically with the spectral code. All these additional modes emerge from the

continuous spectrum. Numerically, the emergence of a discrete eigenmode from the continuous spectrum is first seen as a distortion of the balloon as shown in Fig. 8. This figure zooms in on the birth of such a mode and does not show the entire spectrum. The flow in Fig. 8 corresponds to $G = 2$ (and $l_1 = 0.5$); we note that the pure Couette flow is $G = 0$, while the pure Poiseuille flow is $G = 8$.

7. Numerical results for two-layer flow

We focus on the short wave limit of plane Couette flow. To study this problem we used the representative case $W_1 = 1$, $W_2 = 2$. For two UCM fluids, the entire spectrum is again known. Each fluid has a continuous spectrum as for the one-fluid case. There is a Gorodtsov-Leonov mode at each wall, one for each fluid. In addition there are five interfacial modes [6], four of which are always stable and one of which may be unstable depending on the choice of Weissenberg numbers. In the computations performed here, one of these five eigenvalues is not observed, due to it lying too close to one of the continuous spectra to be resolved. The spectrum (including all five of these modes) is shown in Fig. 9.

As we increase the parameter β and move into the Oldroyd-B regime, we see that each fluid now has a second continuous spectrum, exactly as in the case of a single fluid. Near the new continuous spectra, there are families of new discrete modes. To the right of each spectrum there are up to four modes, appearing in pairs of one interfacial mode with one wall mode. These are

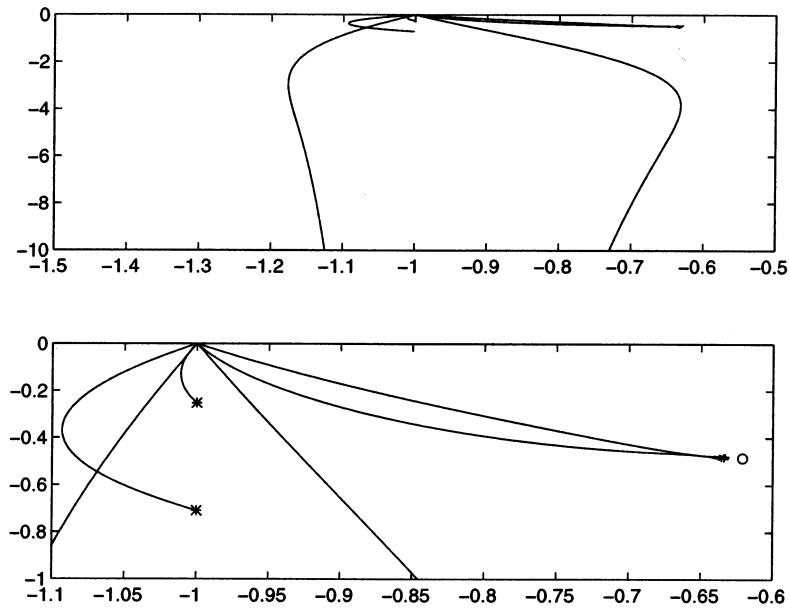

Fig. 7. Motion of the eigenvalues in the σ-plane as α varies: Poiseuille flow of a UCM fluid with $W = 1$. All eigenvalues coincide at -1 at $\alpha = 0$. As α increases, two eigenvalues move to the Gorodtsov-Leonov eigenvalue marked by a circle, two disappear in the continuous spectrum (marked by a star), and two behave like $-i\alpha - 1/W$.

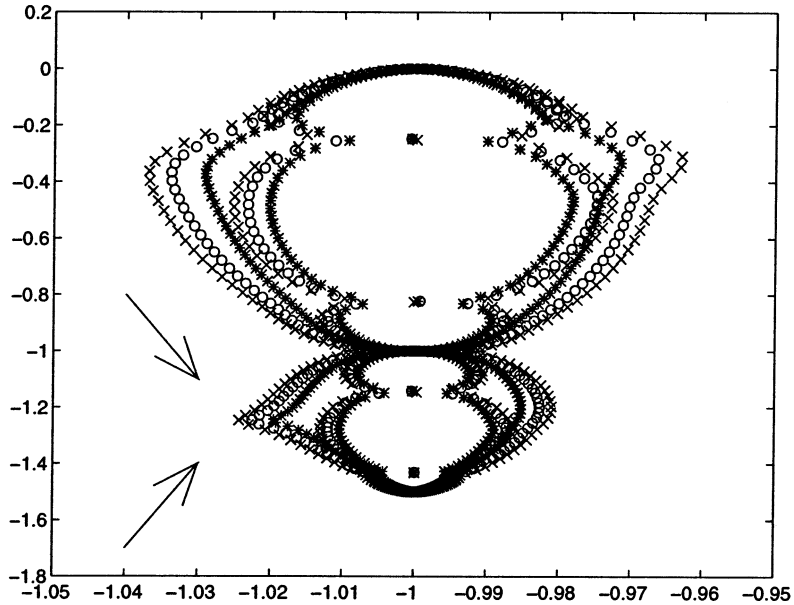

Fig. 8. Emergence of a single mode during transition from Couette to Poiseuille flow for the UCM fluid. Note the distortion of the balloon highlighted by the arrows. As the Poiseuille component of the flow is increased further, a discrete mode emerges in this location. The parameters are $\alpha = 1$, $G = 2$, $W = 1$. Results with 90 (crosses), 100 (circles) and 120 (stars) Chebyshev modes are displayed.

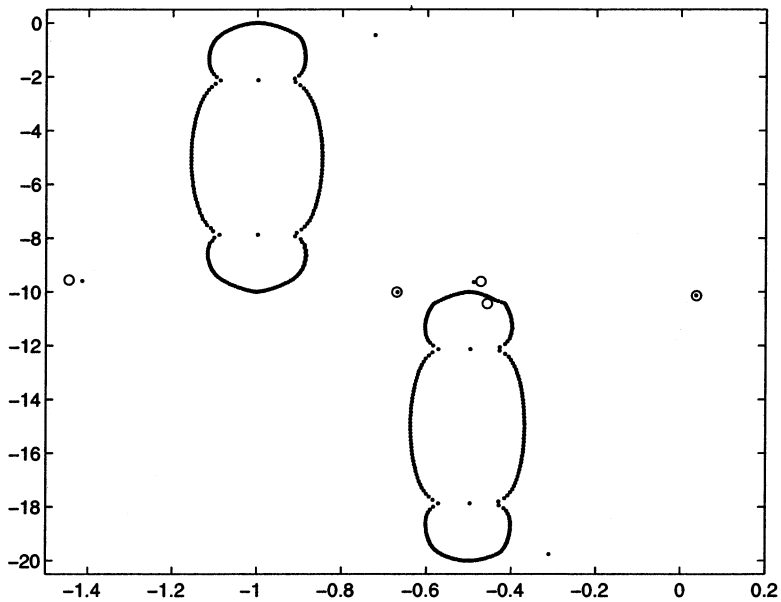

Fig. 9. The spectrum for Couette flow of two UCM fluids (with Weissenberg numbers $W_1 = 1$ and $W_2 = 2$) at wavenumber $\alpha = 10$ (.) together with exact analytical results of the five interfacial modes (o) for the limit $\alpha \to \infty$.

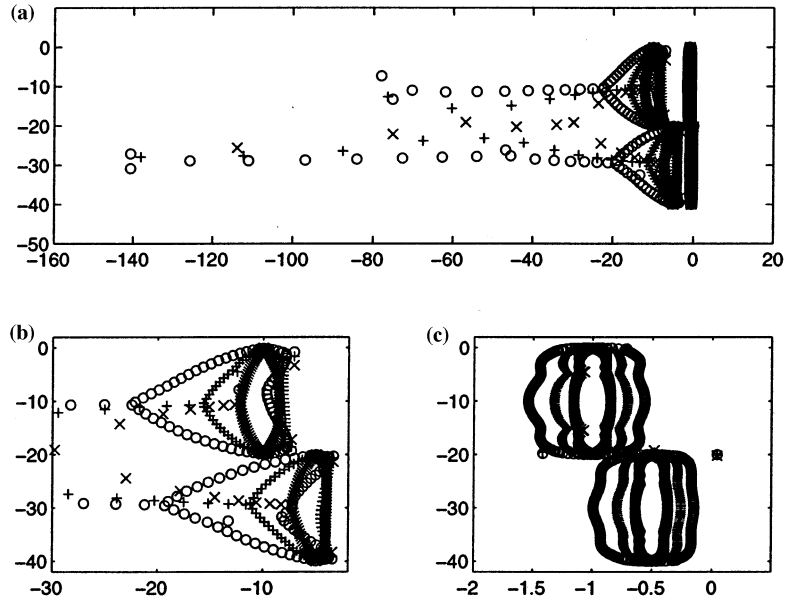

Fig. 10. Spectrum for short waves $\alpha = 10$ (crosses), 20 (plusses), 40 (circles) of two Oldroyd-B fluids in Couette flow. (a) shows the entire spectrum as the wavenumber α varies; (b) and (c) are enlargements showing the 'new' and 'old' (UCM) parts of the spectrum. The parameters are $\beta = 0.1$, $W_1 = 1$, $W_2 = 2$.

analogous to the pair of modes near the top and bottom of the left continuous spectrum in Fig. 4 for the single layer case. The number of these modes (four, two or none) appears to decrease with increasing β. To the left of each spectrum (i.e. decaying faster than rate $1/W\beta$) there is a 'trail' of discrete modes. Their imaginary parts vary slightly, but as the wavelength tends to zero ($\alpha \to \infty$) they all have imaginary part corresponding to the middle of the fluid: neither interfacial nor centred close to a wall. This is shown in Fig. 10.

The number of these modes decreases with increasing, β, but in our case some persist up to $\beta = 0.8$. Beyond this value, as β gets close to 1, the old 'UCM' continuous spectrum in one fluid and the new spectrum in the other fluid are located in close proximity, as evident from Eqs. (15) and (16), and discrete modes in the vicinity become difficult to identify. We have described the trends with β for two-layer flows for short waves. This may be interpreted as a qualitatively representative case for other wavenumbers. For the short wave limit, we have classified several modes as wall modes or interfacial modes because of the fast decay of their eigenfunctions away from the walls and interface in this limit; these will inevitably not be localized for longer waves.

Acknowledgements

This research was supported by the National Science Foundation under Grants DMS-9622735 and CTS-9612308.

References

[1] R. Sureshkumar, A. N. Beris, Linear stability analysis of viscoelastic Poiseuille flow using an Arnoldi-based orthogonalization algorithm, J. Non-Newtonian Fluid Mech. 56 (1995) 151.
[2] M.D. Graham, Effect of axial flow on viscoelastic Taylor-Couette instability, J. Fluid Mech. 360 (1996) 341.
[3] M. Renardy, Y. Renardy, Linear stability of plane Couette flow of an upper convected Maxwell fluid, J. Non-Newtonian Fluid Mech. 22 (1986) 23.
[4] P.G. Drazin, W.H. Reid, Hydrodynamic stability, Cambridge University Press, Cambridge, 1981.
[5] V.A. Gorodtsov, A.I. Leonov, On a linear instability of a plane parallel Couette flow of a viscoelastic fluid, J. Appl. Math. Mech. (PMM) 31 (1967) 310.
[6] Y. Renardy, Stability of the interface in two-layer Couette flow of upper convected Maxwell liquids, J. Non-Newtonian Fluid Mech. 28 (1988) 99.
[7] M. Renardy, A rigorous stability proof for plane Couette flow of an upper convected Maxwell fluid at zero Reynolds number, Euro. J. Mech. B. 11 (1992) 511.
[8] M. Abramowitz, I.A. Stegun, Handbook of Mathematical Functions, Dover, New York 1965.
[9] Y. Renardy, B. Khomami, K.C. Su, M.A. Clarke, An experimental and theoretical investigation of interfacial stability in superposed pressure-driven channel flow of viscoelastic fluids, in preparation.
[10] T.C. Ho, M.M. Denn, Stability of plane Poiseuille flow of a highly elastic liquid, J. Non-Newtonian Fluid Mech. 3 (1977) 179.
[11] H.J. Wilson, J.M. Rallison, Short wave instability of co-extruded elastic liquids with matched viscosities, J. Non-Newtonian Fluid Mech. 72 (1997) 237.